Int J Appl Earth Obs Geoinformation 93 (2020) 102209

Contents lists available at ScienceDirect

Int J Appl Earth Obs Geoinformation

journal homepage: www.elsevier.com/locate/jag

Woody vegetation cover, height and biomass at 25-m resolution across Australia derived from multiple site, airborne and satellite observations

Zhanmang Liao[a], Albert I.J.M. Van Dijk[b,*], Binbin He[a,d], Pablo Rozas Larraondo[b], Peter F. Scarth[c]

[a] School of Resources and Environment, University of Electronic Science and Technology of China, Chengdu, Sichuan, 611731, China
[b] Fenner School of Environment & Society, Australian National University, Canberra, 2601 ACT, Australia
[c] Joint Remote Sensing Research Program, School of Earth and Environmental Sciences, University of Queensland, Brisbane, QLD, 4072, Australia
[d] Center for Information Geoscience, University of Electronic Science and Technology of China, Chengdu, Sichuan, 611731, China

ARTICLE INFO

Keywords:
Tree cover
Vegetation height
Woody biomass
Australia
LiDAR
Landsat

ABSTRACT

Detailed spatial information on the presence and properties of woody vegetation serves many purposes, including carbon accounting, environmental reporting and land management. Here, we investigated whether machine learning can be used to combine multiple spatial observations and training data to estimate woody vegetation canopy cover fraction ('cover'), vegetation height ('height') and woody above-ground biomass dry matter ('biomass') at 25-m resolution across the Australian continent, where possible on an annual basis. We trained a Random Forest algorithm on cover and height estimates derived from airborne LiDAR over 11 regions and inventory-based biomass estimates for many thousands of plots across Australia. As predictors, we used annual geomedian Landsat surface reflectance, ALOS/PALSAR L-band radar backscatter mosaics, spatial vegetation structure data derived primarily from ICESat/GLAS satellite altimetry, and spatial climate data. Cross-validation experiments were undertaken to optimize the selection of predictors and the configuration of the algorithm. The resulting estimation errors were 0.07 for cover, 3.4 m for height, and 80 t dry matter ha^{-1} for biomass. A large fraction (89–94 %) of the observed variance was explained in each case. Priorities for future research include validation of the LiDAR-derived cover training data and the use of new satellite vegetation height data from the GEDI mission. Annual cover mapping for 2000–2018 provided detailed insight in woody vegetation dynamics. Continentally, woody vegetation change was primarily driven by water availability and its effect on bushfire and mortality, particularly in the drier interior. Changes in woody vegetation made a substantial contribution to Australia's total carbon emissions since 2000. Whether these ecosystems will recover biomass in future remains to be seen, given the persistent pressures of climate change and land use.

1. Introduction

Detailed spatial information on the presence and properties of woody vegetation serves various purposes, from land management and planning to nature conservation, fire risk management, and greenhouse gas emissions mitigation and reporting on both sources and sinks. Relevant properties include, in order of increasing complexity: the presence, canopy cover fraction, height, biomass, structure and floristic composition of the woody vegetation component. Ideally, this information is available as a regularly updated time series, allowing it to be used for monitoring, accounting and reporting purposes (van Dijk et al., 2014).

Satellite remote sensing has been shown a cost-effective method for deriving temporal information on forest presence and canopy density over large areas. At the global scale, Hansen et al. (2000) used MODIS optical observations to develop the 'vegetation-continuous fields' (MODIS VCF) product using a machine learning approach. The information was developed using a regression tree ensemble using 250-m MODIS reflectance that was trained on an aggregated 30-m mapping of projected canopy cover using Landsat; itself verified using very high-resolution imagery. Addressing the increase in spatial resolution necessary to monitor the ongoing degradation of global forest stocks, Hansen et al. (2013) developed a Landsat-based binary forest mapping methodology. These global data sets are a valuable resource for global change studies and as a benchmark. However, they have typically traded off resolution to achieve global coverage and do not always make optimum use of regional or national data to constrain estimates, at least in the Australian context. A number of studies have explored the use of single or multiple sensor satellite observations to assess woody vegetation over Australia. The first attempt to repeatedly map forest

* Corresponding author.
E-mail address: albert.vandijk@anu.edu.au (A.I.J.M. Van Dijk).

https://doi.org/10.1016/j.jag.2020.102209
Received 24 April 2020; Received in revised form 26 July 2020; Accepted 30 July 2020
Available online 19 August 2020

cover over Australia was to support the country's National Carbon Accounting System (NCAS; Furby, 2002; Lehmann et al., 2013). The NCAS mapping system continues to operate and uses statistical methods applied to Landsat series observations to map the presence or absence of forest, as defined under the Kyoto protocol. Known disadvantages of the mapping product are its categorical nature, which can be challenged by Australia's extensive low-cover dry woodlands, and the partially counterfactual character of Australia's Kyoto definition of a forest as "*a minimum area of land of* 0.2 ha *with tree crown cover (or equivalent stocking level) of more than 20 per cent with trees with the potential* [sic] *to reach a minimum height of* 2 m *at maturity* in situ". Similarly, the definition of forest used in Australia's National Forest Inventory has been "*An area, incorporating all living and non-living components, that is dominated by trees having usually a single stem and a mature or potentially mature stand height exceeding* 2 m *and with existing or potential crown cover of overstorey strata about equal to or greater than* 20 %", with an operational minimum area threshold of 0.5 ha (pers. comm. S. Read, ABARES). In contrast, operational mapping programmes such as the Queensland Government's Statewide Landcover and Trees Study consider the actual rather than potential presence of woody vegetation, and use a foliage projected cover threshold of 10 % rather than a crown cover threshold. These differences in definitions have contributed to contrasting reports regards trends in forest and woody vegetation more broadly.

Vegetation height and above-ground biomass have proven more challenging to sense remotely. LiDAR measurements are arguably the most reliable method to measure vegetation height, but suitable measurements at global scale were not available until the launch of the Geoscience Laser Altimeter System (GLAS) instrument aboard the ICESat mission launched in 2003. It proved capable of providing global measurements of canopy height (cf. Lefsky et al., 2005; Los et al., 2012; Simard et al., 2011), although the spacing between along-track measurements has limited the accuracy and resolution of vegetation height data.

A comprehensive overview of the development of large-scale forest biomass remote sensing techniques is provided by Lucas et al. (2012). Briefly, vegetation height data from altimetry has provided one approach to estimating biomass, along with active and passive microwave observations (e.g., Baccini et al., 2017; Liu et al., 2015; Saatchi et al., 2011). Lucas et al. (2010) were among the first to explore the use of backscatter by the active L-band ALOS PALSAR radar satellite instrument for biomass estimation and calibrated a conceptual model to field biomass measurements over the state of Queensland. They found that soil moisture had an important confounding influence on backscatter observations, which has since been mitigated by the development of annual PALSAR composites (Shimada et al., 2014). Scarth et al. (2019) developed an approach to integrate the GLAS, PALSAR and Landsat observations for forest structural mapping at 30 m resolution. Except for the low-resolution (~50 km) passive microwave remote sensing approach of Liu et al. (2015), these remote sensing approaches to forest height and biomass mapping have the disadvantage of being derived from active sensors with a short mission life, meaning that they are not suitable for reliable repeated mapping. ESA's twin Sentinel-1 radar imagers do provide an ongoing source of C-band backscatter observations, but given the short wavelength of these observations, the signal may be expected to be more sensitive to the canopy than to total forest biomass.

This study builds on the advances presented but aims to capitalise on some further recent innovations. Firstly, standardised processing of Landsat observations through Geoscience Australia's Digital Earth Australia program has generated a series of annual surface reflectance composites from 1988 onwards (Roberts et al., 2017). So far, these have not been used for forest presence or property mapping. Secondly, a database of spatial vegetation height and fractional cover products over several regions spread across Australia has recently become available and provides a rich database for machine-learning approaches (Fisher et al., 2020; Van Dijk et al., 2018). Our objective was to make optimal use of this expanded range of satellite, airborne and field observations available to produce spatial estimates of woody vegetation cover, height and biomass for Australia at high (25-m resolution). Where feasible, we produced such estimates annually.

2. Data and methods

2.1. Overall approach

Our overall approach was to use Random Forest machine learning algorithms to spatially estimate (1) woody vegetation canopy cover ('cover', WCF as a fraction), (2) vegetation height ('height', VH in m) and (3) woody above-ground biomass ('biomass', WAGB in t dry matter ha^{-1}). The precise definition of these variables is a function of the training data and is described below. Our intent was to estimate annual time series of each variable. This is directly possible for cover, by using only the annual Landsat geomedians as predictors. However, as will be demonstrated, Landsat observations alone do not allow reliable estimation of height and biomass. We addressed this by developing reference estimates for these variables using additional inputs based on GLAS and PALSAR for the period 2007–2010 during which these observations were made.

2.2. Training data

We used cover and height data derived from airborne LiDAR as training data, as well as in situ biomass estimates from a large number of plots. The LiDAR-based vegetation cover and height data are available from the Terrestrial Ecosystem Research Network (TERN)[1] for 11 areas shown in Fig. 1. Some characteristics of the data are listed in Table 1. The LiDAR point cloud data were acquired and processed for TERN following data and methods fully described in Van Dijk et al. (2018). Briefly, data for the ACT was collected at a nominal point density of at least 4 ppm across the region and 8 ppm over the urban area using a Trimble AX60 system containing a Riegl LMS-Q780 laser instrument operated by RPS Mapping, while the remaining sites were mapped at a nominal point density of 6–8 ppm using a Riegl Q560 operated by Airborne Research Australia.

Woody cover fraction (WCF) was defined as the complement of the gap fraction of the canopy above 2 m height, including both woody and leaf canopy elements, calculated following Fisher et al. (2020). These authors compared field observations of canopy gap fraction above 2-m with various candidate metrics calculated from airborne LiDAR collected over 13 Australian sites, including some of those included here. They found empirically that error and bias were minimal when considering all vegetation returns originating from above 1.5 m height, expressed as a ratio over the total number of vegetation and non-vegetation returns. We applied this simple calculation to estimate WCF from the classified LiDAR points at 5-m horizontal grid resolution.

Vegetation height VH was calculated as the median height of the first return of all pulses at 1- or 2-m resolution (van Leeuwen and Nieuwenhuis, 2010). Both cover and height were resampled to 50-m resolution by calculating the median average to generate training data.

Spatially-continuous biomass training data were not available. Instead, we used the Biomass Plot Library, a database of in situ biomass inventories compiled and published by TERN.[2] The database is a collation of stem inventory data collected by different government, university, and industry organisations. Allometric models were used to convert individual tree dimensions to biomass in tonnes of dry matter, which were subsequently aggregated for the full inventory plot. From

[1] all data can be visualised and downloaded via https://maps.tern.org.au

[2] http://data.auscover.org.au/xwiki/bin/view/Product+pages/Biomass+Plot+Library

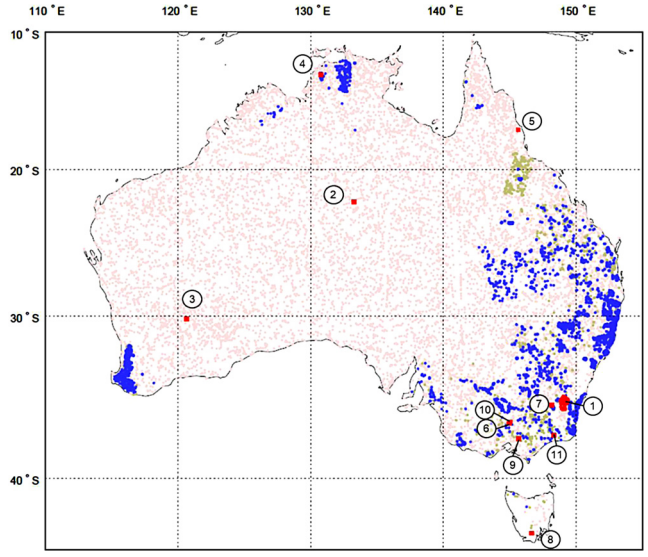

Fig. 1. Location of the airborne LiDAR data (red, numbered cf. Table 1) and of biomass inventory sites that were (blue) and were not (green) included in the training sample, as well as the augmented sample of zero-woody biomass sites (pink). (For interpretation of the references to colour in the Figure, the reader is referred to the web version of this article).

such sites. Therefore, the database was augmented with a large sample of sites without any woody vegetation. We sampled these by combining the national forest presence mapping (Furby, 2002) and MODIS Vegetation Continuous Fields (Hansen et al., 2000) with the cover and height products derived as part of this study. From all locations where all products agreed woody cover was zero and vegetation height less than 2 m, a total of 11,835 samples were drawn, assigned zero biomass and used to augment the woody biomass data.

2.3. Predictors

A primary input to the mapping is an annual time series of Landsat surface reflectance values. Roberts et al. (2017) recently developed an approach to composite repeated Landsat observations over any chosen period into a single higher-dimension geometric median (or geomedian) of internally consistent surface reflectance values. The value of a pixel in a geomedian image is the statistical median of all observations for that pixel from a period of time but calculated in a way that respects the relationship between reflectance in different bands. The product is made available by Geoscience Australia as a 25-m annual geomedian product, based on atmospherically-corrected and cloud-masked Landsat 5, 7 and 8 observations transformed to Australian Albers projection.

Active L-band radar mosaics were used to estimate height and biomass. ALOS PALSAR L-band Fine Beam Dual (HH and HV) polarisation data mosaics are available from JAXA.[3] Shimada et al. (2014)

Table 1
Description of sites with LiDAR-based woody vegetation cover and height data.

Site name	Survey year	Area (km^2)	Training sample	Land cover types
1) Australian Capital Territory	2015	3227	17032	Natural, agricultural, residential
2) Alice Springs (NT)	2014	21	2040	Dry mulga woodland
3) Credo (WA)	2012	22	2220	Dry open woodland
4) Litchfield (NT)	2013	22	2030	Open savannah forest
5) Robson (Qld)	2012	28	5155	Tropical rainforest and pasture
6) Rushworth (Vic)	2012	21	2240	Temperate woodland
7) Tumbarumba (NSW)	2011	24	2699	Humid temperate forest
8) Warra (Tas)	2015	22	2229	Humid temperate forest
9) Watts (Vic)	2012	22	2230	Humid mountain ash forest
10) Whroo (Vic)	2012	0.4	440	Temperate woodland
11) ZigZag (Vic)	2012	22	2270	Temperate forest and open woodland

the full database of 10,823 entries, we rejected those corresponding to plot sizes smaller than 0.03 ha (< 1% of the database), surveyed before 2000 (17 %), and with an estimated absolute or relative uncertainty in field-based biomass exceeding 75 t/ha (4 %) or 25 % (5%), respectively. Visual inspection indicated there were some sites where woody vegetation cover was partially or wholly lost between the survey year and the reference period for biomass estimation. Furthermore, several more sites were temporally stable but located on or near the edge of a transition between woody and non-woody vegetation. In some cases, this might have been due to modest (< 30 m) geolocation errors, whereas in other cases it appeared that the plot shape was very elongated (e.g., being part of a tree belt). To address these issues, we sampled a 3-by-3 neighbourhood around the corresponding pixel in the 25-m gridded WCF estimates derived here, for all years between the survey year and the end of the 2010 reference period. Calculating the spatial mean cover for the common period 2007–2010 between the ALOS/PALSAR and ICESat/GLAS missions as a reference value, we rejected those sites with a spatial standard deviation exceeding 10 % cover (4%); differences between cover for the survey year and reference value exceeding 10 % cover (28 %); and differences between mean cover for the full ICESat/GLAS mission period (2003–2010) and the reference value exceeding 10 % (25 %). The resulting sample size was 5,547, i.e., about half (51 %) of the full database.

Initial training attempts produced overestimates of biomass in non-woody vegetation, most likely because the database did not include any

describe how the data was ortho-rectified, topographically corrected, and intensity balanced during mosaicking. We used both the HH and HV mosaics and calculated average values for the four years (2007–2010), after which they were resampled to 25-m in Australian Albers projection.

The structural vegetation classification for Australia by Scarth et al. (2019) was also used to help estimate height and biomass. The authors first applied image segmentation to the PALSAR and Landsat imagery to create self-similar clusters of pixels (or superpixels). ICESat/GLAS L2 Global Land Surface Altimetry Data for the period 2003–2009 were obtained from the National Snow and Ice Data Centre. These data were processed for differences in footprint size, laser output power, vegetation/ground reflectance, and terrain slope and then aggregated for each cluster into mean vertical profiles. From these, profile height percentiles were extracted for different percentiles (h25, h50, h75, h95 and h100). The metrics for clusters without data were estimated based on similarity criteria. The resulting mapping product is available from TERN[4] . Because PALSAR mosaics were used alongside Landsat in the segmentation and interpolation steps, the structural vegetation classification is not perfectly independent from the PALSAR backscatter data.

[3] https://www.eorc.jaxa.jp/ALOS/en/palsar_fnf/fnf_index.htm
[4] http://data.auscover.org.au/xwiki/bin/view/Product+pages/ICESat+Vegetation+Structure

However, in practice the shared information content is minimal and in any event the machine learning method used is robust against correlation between predictors.

Initial testing made it clear that static spatial data sets of climate variables improved the estimation of forest biomass considerably (see Results). To this end, gridded data on long-term average air temperature, precipitation and radiation were obtained from TERN and from the Bureau of Meteorology (BoM). Specifically, gridded mean air temperature and precipitation at 0.05° based on interpolation of station measurements were obtained from BoM, and mean annual radiation based on a combination of solar radiation and illumination modelling on a 3-arcsecond (~90 m) digital elevation model (Wilson and Gallant, 2000) was obtained from TERN.

The different predictor data sets varied in spatial resolution (25–90 m) and in some cases needed to be reprojected. In training and performance assessment this was allowed for by resampling the predictor and predictands to 50 m and 75 m squared, respectively. The outputs were produced at 25-m resolution, but with the caveat that the spatial accuracy may be somewhat less.

2.4. Methods

We trained Random Forests to predict cover, height and biomass using the spatial input fields. For cover, we used all bands of the Landsat geomedians as candidate predictors. For height, we used these same geomedians, as well as the ALOS/PALSAR mosaics and ICESAT/GLAS vegetation height percentiles. For biomass, we used the average of cover predictions for 2007–2010 and the height predictions derived in the previous steps, as well as the Landsat geomedians, ALOS/PALSAR mosaics and gridded climate data.

When trained on LiDAR-derived cover and height, the predictors were resampled to the same 50-m grid as the resampled LiDAR products, after which a regularly-spaced sparse sample was taken to limit computational costs. The sample represented 1.3 % of the available data for the ACT ($N = 6838$) and close to 25 % ($N \sim 2000$) for the other, smaller grids. This produced a total sample size of N = 40,585. Regression modelling requires that the data distribution is approximately Gaussian. This was the case for cover and height, but the biomass data were positively skewed (skewness 2.37). Taking the cube root made these data close to normally distributed (skewness 1.04).

2.5. Model

The 'TreeBagger' function in MatLab was used. Experiments were carried out with two- to eight-fold cross-validation (and all integer values in between) to determine the most robust model configuration and selection of predictors, using the root mean square error (*RMSE*) as the selection criterion. The number of leaf nodes was varied from 5 to 50, and the ensemble size from 5 to 500.

To understand the contribution of each of the predictors to performance, mean importance was calculated for k out-of-bag predictor importance sets returned by the algorithm in k-fold cross-validation. We carried out predictor removal experiments to determine the optimal number and set of predictors, in which the algorithm was initially trained with all available predictors and successively retrained, each time removing the least important remaining predictor. The experiment was repeated three times and the set of predictors that consistently outperformed the others was selected.

Generalised empirical response functions between each predictor (x_i) and the predictand (y) were visualised by calculating the median and interquartile range of y for equal x_i intervals between the 2% lowest and 2% highest x_i values (see Fig. 2b for an example). An interquartile range that is narrow compared to the range of median values indicates a strong relationship between x_i and y. The same visualisation was made using predicted values (y_{est}) instead of y. For a reliable prediction, it would be expected that the median and interquartile patterns for y and y_{est} overlap.

2.6. Evaluation

Validation performance was evaluated using the withheld sample data from the k-fold trials. The *RMSE*, the coefficient of determination (R^2), bias and model efficiency *ME* (Nash and Sutcliffe, 1970) were calculated as measures of performance. The value of *ME* is mathematically equal to R^2 if there is no systematic bias in the predictions and lower if there is. The final predictions (i.e., not those used for validation) were made with an algorithm trained on the full training data set. For cover and height, we also evaluated performance for individual LiDAR capture areas using the full dataset collected.

We analysed the agreement and differences between the cover estimates and alternative vegetation cover products. These included the MODIS VCF product, Normalised Difference Vegetation Index (NDVI), and a Photosynthetic Vegetation cover fraction. MODIS VCF for the year 2015 was reprojected and resampled to 500-m resolution, and compared to WCF for the same year and at the same resolution.

The Normalised Difference Vegetation Index (NDVI) has frequently been used to estimate fractional canopy cover (FC) and the closely related fraction of absorbed photosynthetic radiation (*FPAR*, often assumed 0.95 times *FC*). To do so, NDVI is commonly linearly scaled between values of ca. 0.10–0.15 and ca. 0.80–0.85, assuming that a maximum FC of 0.95 is achieved for the latter. NDVI was calculated from the geomedian reflectances.

Guerschman et al. (2015) developed a method to estimate the respective projected fractions of photosynthetic vegetation (PV, i.e. living leaves), non-photosynthetic vegetation (wood and litter) and bare soil from Landsat reflectance. The respective fractions are produced operationally and available through Geoscience Australia. We composited the individual images to bi-monthly median values, and the lowest value (minPV) of the six intervals was compared to WCF. The expectation was that there would be a correlation between our estimated WCF and MODIS VCF, NDVI and minPV, but that NDVI and minPV would generally exceed WCF due to the contribution of short vegetation. The strongest correlation was expected with MODIS VCF, as it represents woody canopy cover only, similar to our definition of WCF. The weakest correlation was expected for NDVI. An intermediate correlation was expected between WCF and minPV, as short herbaceous vegetation tends to senescence at some stage during the year across most of Australia, although with some notable exceptions.

The LiDAR-derived and predicted cover were also compared to the categorical NCAS forest mapping product. Our interest was to determine whether a cover threshold could be found and applied to the LiDAR-observed and predicted cover data to closely match the categorical NCAS mapping, and to interpret any differences that occurred. The NCAS mapping product contains three classes (non-forest, sparse woodland and forest), intended to correspond to cover thresholds of 10 % and 20 %, respectively. Four of the LiDAR areas had sufficient non-forest and forest for a comparison. For the purposes of comparison we merged the sparse woodland class with the non-forest class. We used LiDAR cover to identify the cover threshold for each site that produced the highest rate of agreement, calculated as the fraction of pixels classified correctly. We subsequently applied these site-specific thresholds to the cover product. We also applied pre-determined thresholds of 10 % and 20 % for comparison.

Finally, continental predictions of cover, height and biomass were made, in the case of cover for the period 2000–2018, by distributed processing on high-performance computing infrastructure. These were analysed for consistency with known spatial and temporal patterns of woody vegetation cover, height and biomass.

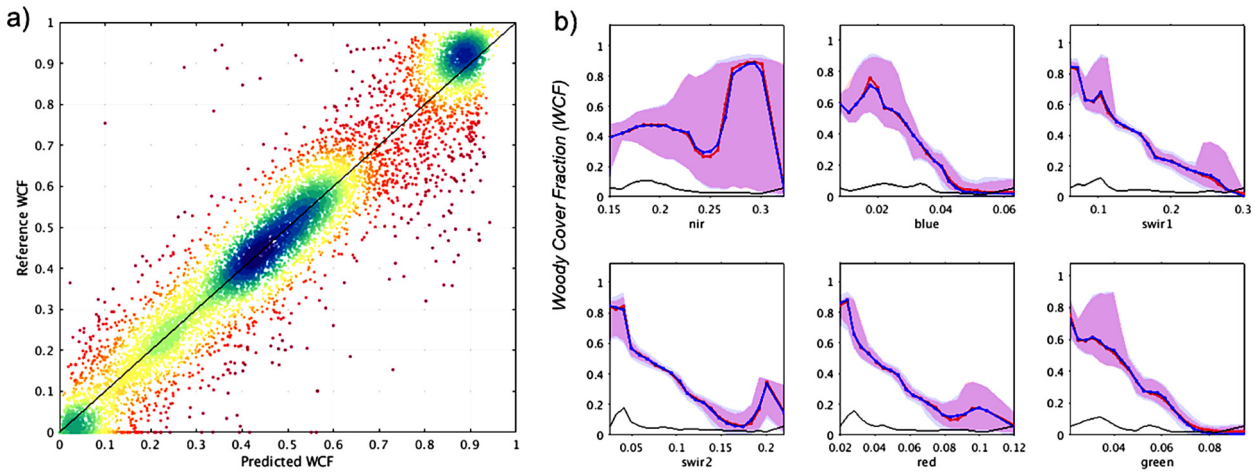

Fig. 2. (a) Scatter plot of predicted vs. reference Woody Cover Fraction (WCF, as fraction) for validation coloured from low (red) to high kernel density (blue) (only half of the data pairs are shown for visualisation purposes). (b) Plots showing the distribution of in situ (blueish colours) and predicted (reddish colours) cover as a function of each predictor (reflectance as a fraction), shown in order of decreasing prediction importance. Shown are the median (line) and inter-quartile range (band) for equal predictor intervals; purple colours indicate overlapping ranges. Also shown the sample size for each interval (black line, no scale). (For interpretation of the references to colour in the Figure, the reader is referred to the web version of this article).

3. Results

3.1. Model configuration

In all three cases, we found that calibration and validation performance converged and stabilised if an ensemble of 50 or more was used in combination with 20 leaves per node, regardless of the *k*-fold sample split chosen. For cover and height, there was no appreciable change in validation performance from two- to eight-fold cross-validation. We interpreted this to be because the training sample was sufficiently large for half of the sample to contain most of the variation present in the population. In the case of biomass, the eight-fold validation RMSE was 4 % smaller than the two-fold validation performance. We interpret this to indicate a risk that the eight-fold cross-validation model might have been overfitted to some degree, and selected four-fold cross-validation, which showed near-identical performance, to reduce that risk. In the remainder of this section, we refer to results obtained with a Random Forest ensemble of 100 with a minimum 30 leaves per node, applied in two-fold (for cover and height) or four-fold (for biomass) cross-validation.

3.2. Performance and predictors selected

The performance measures achieved are listed in Table 2. The R^2 and ME values were identical, which means that the model was free of any bias. For the biomass values transformed back to their original units, the ME value was still very close to R^2, suggesting that the transformation did not lead to a large bias.

The predictor removal experiments for cover and height showed that all candidate predictors made a meaningful contribution to validation performance, although the contribution of *h25* and *h100* to height predictions was marginal. For biomass, the complete set of 18 variables (6 geomedian reflectance, 5 LiDAR heights, 2 radar variables, 3 climate variables, and WCF and VH) did not provide the optimal results. RMSE slightly improved as variables were successively removed, achieving a 4.1 % improved RMSE when only five variables remained. Removing these remaining variables (Rad, Rain, WCF, VH, and finally Temp) did degrade performance. Therefore, the five variables were retained in the selected model.

3.3. Woody canopy cover fraction

The RMSE for predictions of cover was 0.072 and ME was 0.94 (Table 2). A comparison of predicted and LiDAR-derived cover data pairs (Fig. 2a) suggests a good predictive ability for most of the dynamic range, but there was evidence of slight underestimation over nearly closed canopy (e.g., WCF > 0.85). With the exception of near-infrared (NIR) reflectance, empirical relationships between reflectance and cover resembled a ramp function with low and high reflectance corresponding to high and low cover, respectively (Fig. 2b). A more complex and less well-defined relationship was found between NIR and cover. Interpreting these relationships, a combination of high NIR reflectance and low reflectance in the other bands leads to a high cover estimate, whereas alternative combinations produce a lower cover prediction. The predicted relationships and ranges corresponded well with the empirical relationships derived from the LiDAR observations (overlapping lines and shaded areas in Fig. 2b).

A comparison of performance statistics between sites produced a similarly small bias and RMSE as for the full dataset (see Supplementary Material for figures for each site). The worst performance was found for site 9. This could partially be attributed to the fact that the very high cover over this tall mountain ash forest could not be reproduced, and partly to the moderate spatial variance at this site (Table 3).

Table 2
Performance of the trained random forest ensemble in terms of root mean square error (RMSE), coefficient of determination (R^2) and Nash-Sutcliffe model efficiency (ME). Also listed is the total sample size (N) and the predictors used in order of decreasing importance. WAGB* denotes performance for the estimates transformed back to t ha^{-1} and considering the in-situ woody biomass data only, rather than the augmented data set.

Variable	*RMSE*	R^2	*ME*	*N*	Variable importance order
WCF (fraction)	0.0715	0.940	0.940	40,585	*nir, blue, swir1, swir2, red, green*
VH (m)	3.35	0.889	0.888	40,585	*blue, nir, swir1, HV, swir2, green, red, HH, h95, h75, h50, h25, h100*
WAGB (t ha^{-1})$^{1/3}$	0.667	0.927	0.927	16,681	*Temp, VH, WCF, Rain, Rad*
WAGB* (t ha^{-1})	79.8	0.519	0.494	5546	(as above)

Table 3
Description of sites in terms of LiDAR-derived median and 95 % range of woody cover fraction (WCF) and measures of prediction performance: prediction bias, root mean square error (RMSE), coefficient of determination (R^2) and model efficiency (ME). Note: all cover values are given in % to reduce the number of digits.

Site name	median (95 % range)	bias	RMSE	R^2	ME
1) Australian Capital Territory	37 (0 – 71)	0.3	7.3	0.90	0.90
2) Alice Springs (NT)	36 (26 – 43)	−1.1	3.5	0.56	0.42
3) Credo (WA)	18 (6 – 33)	0.3	4.2	0.63	0.62
4) Litchfield (NT)	24 (15 – 36)	0.2	4.4	0.41	0.40
5) Robson (Qld)	92 (0 – 98)	−0.8	8.2	0.91	0.91
6) Rushworth (Vic)	43 (31 – 49)	−0.3	3.4	0.70	0.70
7) Tumbarumba (NSW)	52 (25 – 70)	1.4	7.1	0.62	0.61
8) Warra (Tas)	91 (50 – 96)	−1.7	9.0	0.34	0.32
9) Watts (Vic)	86 (66 – 94)	−3.6	9.1	0.12	−0.41
10) Whroo (Vic)	42 (36 – 47)	−0.8	2.7	0.24	−0.05
11) ZigZag (Vic)	59 (44 – 82)	1.8	8.1	0.35	0.23

3.4. Vegetation height

The RMSE for height predictions was 3.4 m and ME was 0.88 (Table 2). A comparison of predicted and LiDAR-derived height data pairs (Fig. 3a) suggests some saturation for tall forests, in that the height of vegetation taller than ~40 m was frequently underestimated. Generally, estimation errors increased with vegetation height, i.e., errors were heteroscedastic and partly proportional to the estimate.

Empirical relationships between Landsat surface reflectance and GLAS height and VH were broadly similar to those with cover, but with greater scatter. The relationship between PALSAR radar backscatter and height conformed to expectation, although the non-monotonic relationship for HH polarisation backscatter was not. The relationship between GLAS and LiDAR height was monotonic and near-linear as expected. Predicted height most closely approached h_{75} (i.e. the height below which 75 % of the GLAS returns originated) (Fig. 3b).

Performance statistics for individual sites showed a bias within 1 m and an RMSE similar or less than the full dataset for most sites, except for the sites with the tallest forests (8 and 9, Table 4). In both cases, the predictions could not fully reproduce the large height variations (> 20 m) over short distances (see Supplementary Material).

Table 4
Description of sites in terms of median and 95 % range of vegetation height (VH in m) and measures of prediction performance (acronyms as for Table 3).

Site name	median (95 % range)	*bias*	*RMSE*	R^2	*ME*
1) Australian Capital Territory	5 (0 – 17)	0.4	2.7	0.68	0.67
2) Alice Springs (NT)	3 (2 – 4)	0.1	0.5	0.20	0.11
3) Credo (WA)	6 (3 – 8)	−0.3	1.0	0.33	0.26
4) Litchfield (NT)	8 (4 – 12)	−0.7	1.7	0.48	0.38
5) Robson (Qld)	26 (0 – 32)	−0.4	3.3	0.85	0.85
6) Rushworth (Vic)	12 (10 – 15)	−0.1	1.6	0.12	0.01
7) Tumbarumba (NSW)	22 (13 – 32)	0.0	3.8	0.54	0.53
8) Warra (Tas)	27 (9 – 38)	1.2	6.1	0.36	0.34
9) Watts (Vic)	38 (19 – 55)	−3.0	8.2	0.32	0.21
10) Whroo (Vic)	16 (15 – 17)	−0.7	1.3	0.06	−1.00
11) ZigZag (Vic)	17 (12 – 25)	−0.3	2.6	0.46	0.45

3.5. Woody above-ground biomass

The RMSE for biomass predictions was 80 t ha^{-1} and ME was 0.49 (Table 2). A comparison of predicted and field-measured data pairs (Fig. 4a) suggests saturation at high biomass. However, this effect is much less in the transformed data and therefore, can be attributed primarily to the non-Gaussian distribution of the biomass data. Indeed, under- and overestimations at high biomass were similarly frequent (Fig. 4a). As a logical consequence of the back-transformation, the estimation error increases with biomass.

The empirical relationships between biomass, cover and height were as expected, that is, biomass monotonically increased with both variables (Fig. 4b). The relationship with mean temperature (*Temp*) was also as expected, with the highest biomass found at cool sites. The decrease in biomass with local mean radiation (*Rad*) may be because higher radiation broadly coincides with higher temperature in Australia. The increase in biomass with precipitation (*Rain*) and stabilisation around 800 mm y^{-1} rainfall agreed with expectation, but the subsequent decrease did not.

3.6. Continental mapping

Continental predictions of cover, height and biomass for the period 2007–2010 show strong commonalities in spatial patterns (Fig. 5). Notable differences are the more localised occurrence of tall (> 30 m)

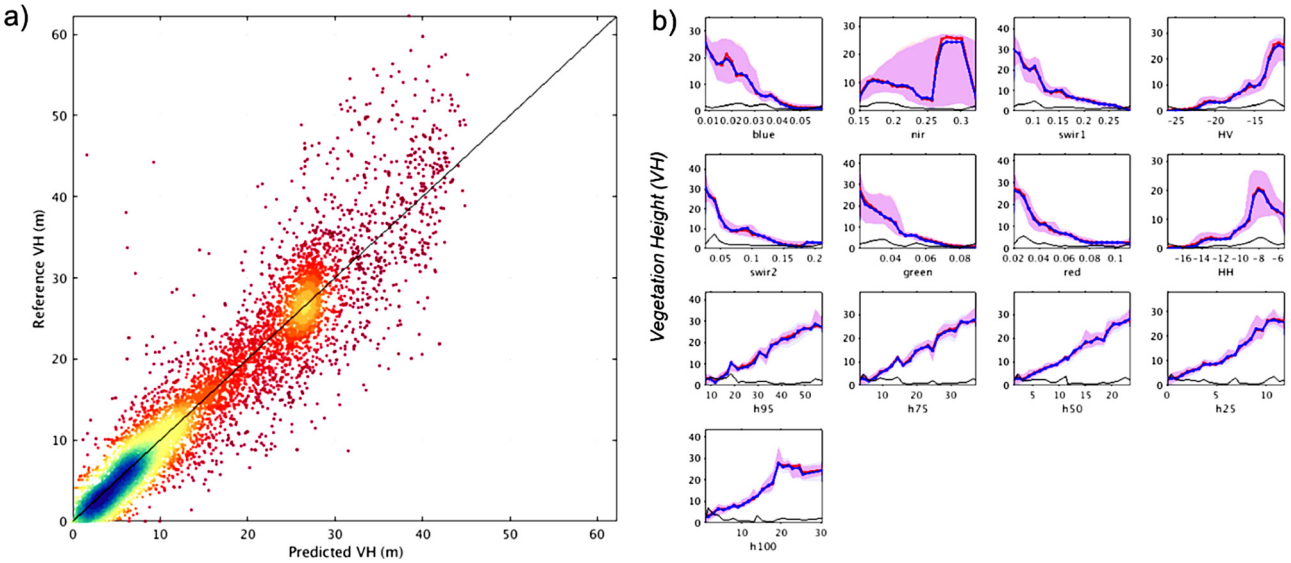

Fig. 3. As Fig. 2 but for vegetation height (VH in m). Units are fraction for Landsat reflectances (red, green, blue, nir, swir1, swir2), dB for PALSAR (HV and HH) and m for altimetry (h_{25}, h_{50}, h_{75}, h_{95} and h_{100}). (For interpretation of the references to colour in the Figure, the reader is referred to the web version of this article).

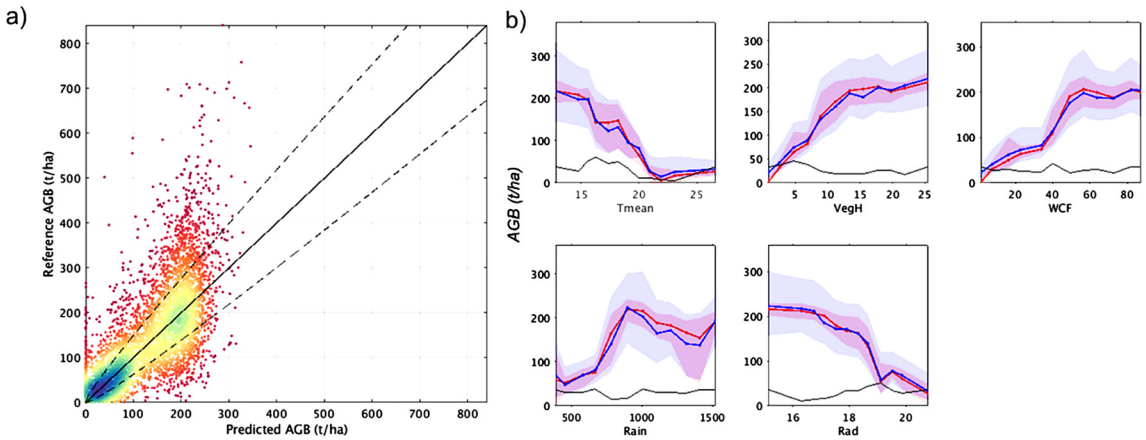

Fig. 4. As Fig. 2 but for woody above-ground biomass (AGB in t/ha); dashed lines in (a) indicate the standard error of the estimate. Predictor-predictand relationships are for mean annual rainfall (Rain in mm), VH (m), WCF (fraction), mean annual temperature (T_{mean} in °C) and mean daily radiation (Rad in MJ m^{-2}).

forests when compared to the spatial pattern of high cover values. Biomass broadly follows cover and height patterns but is greater in the southern half of the continent.

3.7. Comparison with alternative vegetation cover measures

Our cover estimates showed reasonable agreement with MODIS VCF woody canopy cover fraction (Fig. 6). MODIS VCF values were within 0.1 units of our WCF estimates for 71 % of all grid cells with WCF > 10 % and within 0.2 units for 95 % of grid cells. MODIS VCF values were generally somewhat lower than WCF values across most of its range (Fig. 6).

A comparison between LiDAR-derived cover and NDVI for the 11 LiDAR sites confirms our expectation that NDVI and minPV values would exceed our cover estimates due to the short vegetation component included in the former two (Fig. 8a). Minimum bi-monthly PV values were typically lower than NDVI and closer to cover, but still higher for low cover and, less expected, lower for high cover values (Fig. 8b).

Four of the LiDAR sites had a sufficiently large sample of both forest and non-forest vegetation in the NCAS mapping product for comparison with cover (Table 5). Thresholds that maximise the agreement between the LiDAR-derived cover and NCAS mapping varied from 0.12 to 0.40. When applying the site-specific threshold optimised for NCAS to predicted cover, the latter still produced a better classification result for three out of four sites. If uniform thresholds of 10 % or 20 % cover were used, our cover predictions provided better classification results than NCAS in all cases.

4. Discussion

4.1. Basis for prediction

The six Landsat bands available could be used to predict the presence and cover fraction of woody vegetation with good accuracy. The information content of the NIR band was notably different from that in the other six bands, which all appeared to show rather similar inverse relationships to cover. In the exploratory stage of this research, we calculated and used various spectral indices used to classify woody vegetation or forests proposed in previous studies. However, a Random Forests model using these predictors instead of, or in addition to, the original reflectance showed marginally worse validation performance than the configuration used here. This may be due to the larger number of predictor variables, which can degrade prediction performance if the information content between variables is strongly overlapping. A potential downside of the use of 'raw' reflectance is the potential effect of any topographic shadows that remain in the radiometrically-corrected annual geomedian reflectances. We did not find evidence that this caused errors in the cover estimates. We hypothesise that the Random Forest algorithm structure is able to account for differences in illumination, which affects reflectance in all bands.

The prediction of height required a combination of optical, radar and LiDAR altimetry-derived information. Experiments using only a subset of these inputs produced degraded performance. Conversely, the performance of biomass predictions benefited from the removal of redundant variables. We hypothesise that this was due to correlations between cover, height, and the original observations from which they were derived. To test this, we calculated Spearman's non-parametric correlation between each combination of predictors, using the values included in the biomass training set. These correlation values were used to construct a cluster dendrogram, showing the relationship between predictor variables (Fig. 7). We found that all altimetry-derived measures were highly correlated, as were the two PALSAR-derived predictors and all Landsat bands except NIR. WCF was not most strongly correlated to the Landsat reflectance it was derived from but closer related to radar and altimetry-derived predictors. We attribute this to the ability of the WCF algorithm to retrieve canopy structure information from the combination of contrasting visible/SWIR vs. NIR responses to canopy cover (Fig. 2). Furthermore, VH was more strongly correlated to the radar than to the altimetry observations, which corresponds with the greater importance of the PALSAR rather than altimetry observations in predicting VH (Fig. 3). We assume this to be a result of the necessary extrapolation of relatively sparse ICESat/GLAS measurements, compared to the greater density of the PALSAR observations. Future work to include GEDI mission observations should provide new opportunities to test this assumption.

4.2. Sources of error and uncertainty

The agreement between LiDAR- and satellite-derived cover estimates was generally robust with low bias, but some sources of differences could still be identified. These were found to originate from both data sources. The geomedian reflectance represented an annual average and was not necessarily representative for canopy cover at the time of LiDAR acquisition, though we did not find cases where this clearly affected the results. Artefacts were visible for mixed pixels containing both vegetation and water, where the lower reflectance of the water background appeared to produce potential overestimates of cover. Some evidence was found in the mapping shown in the Supplementary Material to suggest erroneous results for woody vegetation likely to be shorter than 2 m, such as new plantations and dense shrubland. In those cases, the LiDAR-derived cover would be zero, but if the spectral

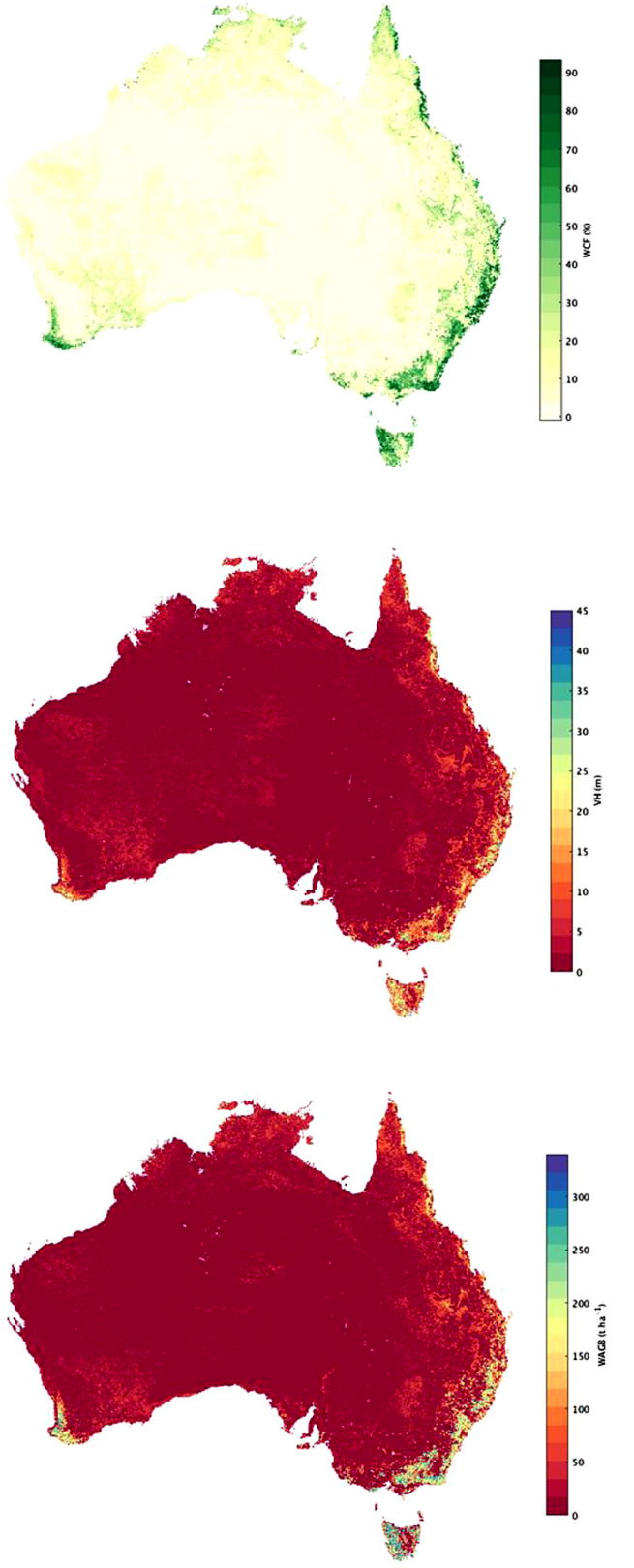

Fig. 5. Continental maps of estimated (top) woody cover fraction (WCF), (centre) vegetation height (VH), and (bottom) woody above-ground biomass (WAGB), all representing the period 2007–2010.

Landsat signature was very similar to that of a forest, a non-zero cover was predicted.

There will also have been error and bias in the LiDAR-derived cover

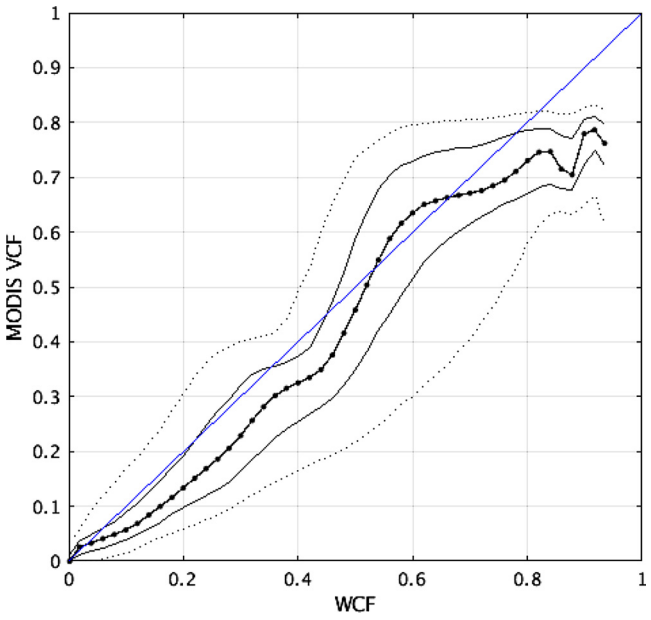

Fig. 6. Relationship between woody-vegetation cover fraction (WCF) derived here and the MODIS Vegetation Continuous Fields (VCF) product, both for 2015 and resampled to 500-m across the continent. For each 0.02 WCF interval, the median (connected dots), interquartile range (solid lines) and 90 % range (dotted line) were calculated.

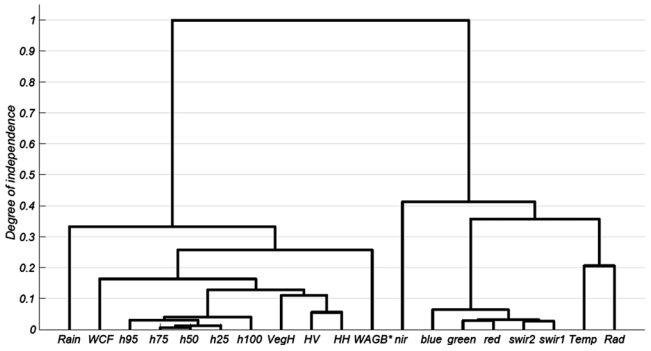

Fig. 7. Cluster dendrogram showing the correlation between variables in the full training dataset used for biomass prediction. WAGB* refers to the plot measurements, whereas WCF and VH refer to predicted values.

estimates. Firstly, the identification of points in the full waveform requires a clear peak intensity. This is more likely to occur in open vegetation with distinct layering than in dense and uniform vegetation, and this introduces a degree of uncertainty into the cover estimates. Secondly, LiDAR pulse density and footprint varied between sites. The specified target pulse density varied from 4 to 8 ppm between sites and within the ACT site. Lower pulse densities can be achieved by higher flight altitudes, and assuming that the LiDAR beam divergence did not change between flights, the LiDAR footprint would have been larger and more diffuse for lower pulse densities. The achieved density of returns also varied widely, from less than 4 to more than 20 ppm, as a result of changes in flight speed and overlapping acquisitions from adjoining flight lines. The above factors lead to inhomogeneity between and within sites. Nonetheless, Fisher et al. (2020) used partly the same LiDAR data as we used, with the same inhomogeneities. Proposing the same calculation also applied here (i.e., the fraction of all LiDAR returns that originate from above 1.5 m height) they achieved an accuracy of ~0.06 when compared to in-field measurements under the canopy. This accuracy is numerically similar to the agreement between LiDAR- and Landsat-derived cover found here.

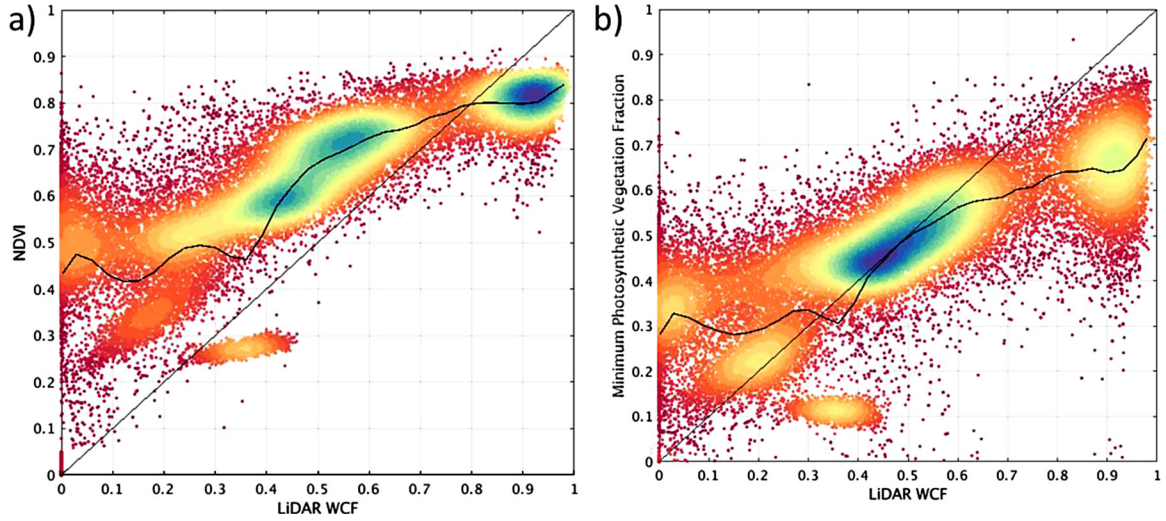

Fig. 8. Density scatter plots showing the relationship between LiDAR-derived woody-vegetation cover fraction (WCF) and (a) the Normalised Difference Vegetation Index (NDVI) derived from the annual Landsat reflectance geomedians; (b) the minimum of bi-monthly average Photosynthetic Vegetation cover fraction derived following Guerschman et al. (2015).

The main challenge for height estimation and the primary source of error were its indirect relationship with optical and radar observations and the low spatial density of GLAS altimetry observations. The predictive performance of Landsat reflectance appeared to be due mainly to the increasing optical darkness associated with taller forests. The predictive performance of L-band radar is assumed to be due to the increased biomass and presence of large reflectors in taller forests. Both are indirect relationships not directly attributable to vegetation height, and both appeared to saturate at heights of 20–30 m. By comparison, altimetry can provide a more direct estimate of vegetation height, but there the challenge was the extrapolation of sparse along-track measurements to pixels without any observations. Although the optical- and radar-based segmentation approach developed by Scarth et al. (2019) is an innovative solution to the sparse nature of the data, it cannot fully avoid uncertainties due to the extrapolation. Among the different ICESat/GLAS percentiles, LiDAR vegetation height most closely resembled h_{75}, that is, the height below which 75 % of the GLAS returns originated. That VH did not correspond to the highest canopy elements (e.g., h_{95} or h_{100}) may be because the height derived initially from the LiDAR represented the median of first returns. This likely resulted in a value closer to Lorey's mean height rather than maximum height.

For biomass, the main challenge was the still relatively small number ($N = 5546$) of in situ estimates available for training, and the wide range of biomass for tree stands with identical height and canopy cover. This wide range partly could be explained by climate controls, and mean temperature in particular. The greater biomass of cooler forests is well known and can be attributed to lower turnover rates (Keith et al., 2009). However, after accounting for temperature and other climatological factors, a relatively large error (RMSE 80 t ha^{-1}) remained. Apart from the limitations of the available predictors, these differences may partly arise from the training data itself. The database represented a collation of site observations from many different sources, determined by varying methods and allometric relationships, each with biases and errors of their own. Some of the differences between predicted and in situ observations could be attributed with confidence. Among the clearest discrepancies, we predicted a very small or zero biomass for some sites where relatively high biomass values (e.g., WAGB > 50 t ha^{-1}) were reported. Visual inspection showed that many of these sites were with tree plantings that were sufficiently large in total area to be included in the training data, but were in effect narrow plantings (e.g. tree belts) too narrow for the surrounding 75 × 75 m pixel region to be representative, despite our best efforts to exclude such sites. Other sites coincided with sparse riparian forests in dry regions. We hypothesise that the use of rainfall as a predictor may have led to an underestimation of the growth potential for these ecosystems, which receive additional water inputs. This illustrates the risk of using predictors that have an environmental but no direct physical connection to biomass. The considerable unexplained variation for high-biomass forests was probably partly related to the underestimation of height, but otherwise could not be attributed with confidence. We hypothesise that age, species composition and ecological history, including fire disturbance, may all be responsible for the unexplained variation.

Explicit consideration of disturbance history, e.g. derived from the cover estimates presented here, may help improve the estimation of height and biomass. More immediately, the recent Global Ecosystem Dynamics Investigation (GEDI) mission can be expected to shine a new light on the underlying reasons for the remaining unexplained variation

Table 5
Comparison of binary forest presence mapping performance between the national NCAS mapping product (Furby, 2002) and thresholding the cover predictions developed in this study, evaluated against LiDAR-derived cover at four sites. Listed are the probability of correct classification (P) and the LiDAR-derived forest percentage (f_{for}) when using that threshold. Also listed are the site-specific threshold of LiDAR-based cover (WCF_{lim}) producing the highest P_{NCAS} at each site.

Site	site-specific WCF_{lim}				WCF_{lim} = 0.20			WCF_{lim} = 0.10		
	WCF_{lim}	P_{NCAS}	P_{WCF}	f_{for}	P_{NCAS}	P_{WCF}	f_{for}	P_{NCAS}	P_{WCF}	f_{for}
1) ACT	0.36	0.82	0.86	49%	0.65	0.85	66%	0.71	0.81	75 %
3) Credo	0.12	0.36	0.34	80%	0.17	0.66	37%	0.00	0.11	90 %
4) Litchfield	0.26	0.38	0.50	41%	0.17	0.29	81%	0.15	0.14	100 %
5) Robson	0.40	0.95	0.97	84%	0.90	0.95	87%	0.89	0.92	88%
mean	0.29	0.63	0.67		0.47	0.69		0.44	0.49	
± st.dev.	± 0.12	± 0.3	± 0.3		± 0.37	± 0.29		± 0.43	± 0.43	

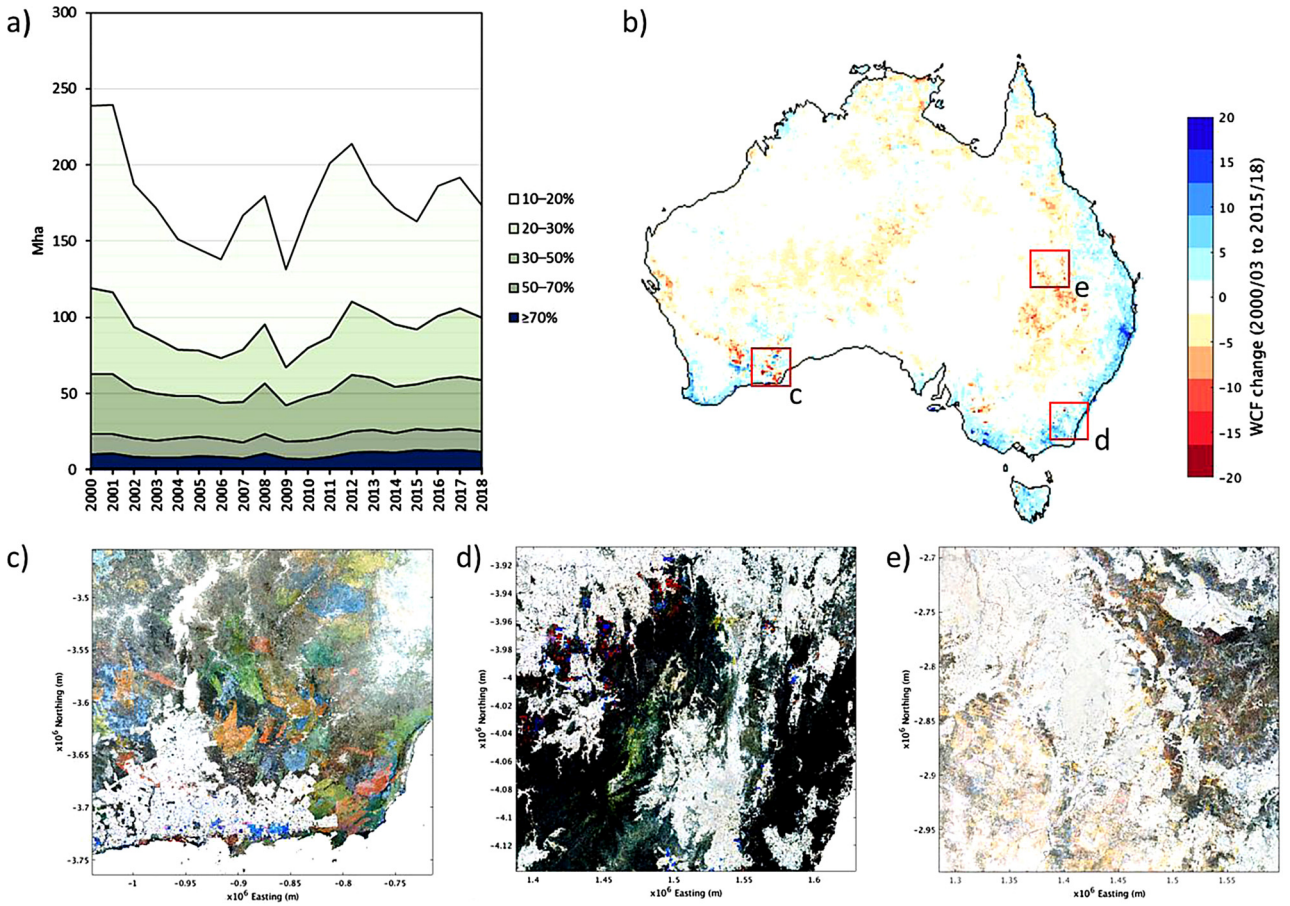

Fig. 9. Temporal change in total woody vegetation cover across Australia (a) annual time series of total extent (in millions of ha, Mha) for different cover thresholds; (b) change in woody vegetation cover between 2000 − 2003 and 2015 − 2018 averaged at 25-km resolution; (c–e) false colour composites of temporal cover dynamics for three regions shown in (b); colours indicate low or absent mean cover for the periods 2015-2018 (red), 2000-2003 (blue) and the entire period (2000-2018), respectively (The colour scales were stretched between 0 and 50 % cover for visualisation purposes). Interpretation is as follows: grey shades indicate stable cover, red hues recent vegetation losses, yellow losses earlier in the period, blue recent gains, green losses followed by recovery, and purple initial gains followed by losses. (For interpretation of the references to colour in the Figure, the reader is referred to the web version of this article).

in height and biomass, and provide opportunities to improve the estimates.

4.3. Trends in Australian woody vegetation cover and biomass

The cover time series was used to analyse temporal changes of woody vegetation cover on the Australian continent. For each year, we calculated the total extent of woody vegetation for different cover thresholds (10, 20, 30, 50 and 70 %) at 25-m resolution (Fig. 9).

For the period 2000–2018, the total area of woody vegetation with ≥50 % cover (including open and closed forests conform Australia's National Forest Inventory) was 25.3 Mha or 3.3 % of the total land surface area (771 Mha). However, choosing a threshold of 10 % increased the area to 173.4 Mha (22.5 %). As much as 69 % of the land area appeared to have at least some woody vegetation at 25-m resolution (> 1 % cover), although we expect this number to be biased high due to estimation error at very small cover values. Temporal fluctuations occur regardless of definition (Fig. 9a). These changes are well-understood and attributable to multi-annual cycles in water availability, with a gradual decline during the Millennium Drought (2001–2009), recovery due to the 'Big Wet' (2010–2011) and a subsequent decline due to a return of dry conditions (van Dijk et al., 2013). They are superimposed on a long-term declining trend (2000 − 2018) due to ongoing land clearing, but the long-term trend varies as a function of threshold. A large −39 % or 46 Mha decrease was calculated for sparse woodlands and shrublands (10–20 % cover), as well as a −22 % or 21 Mha decrease for woodland forest (20–50 % cover), but contrasting with an 8% or 2 Mha increase in open and closed forests (> 50 % cover; Fig. 9). Clearly, the definition of woody vegetation cover has significant consequences for calculated extents, trends and inferences derived from them.

At the national scale, woody cover gains during the 2000–2018 period dominate in many of the coastal regions, whereas losses dominate inland (Fig. 9b). Detailed colour composites illustrate the driving processes (Fig. 9c-e): the planting and harvesting cycles of plantation forestry (strong red and blue hues); the impact of bushfires at different times (patches in multiple colours with sharp boundaries) and the effects of land clearing and drought mortality in more sparse vegetation (light yellow and pink hues).

Estimating the changes in biomass associated with these processes would be valuable, e.g. for understanding the contribution of Australia's ecosystems to the global carbon cycle. This requires assumptions, because here we were only able to estimate mean biomass for the reference period 2007–2010. An approximate estimate may be obtained by multiplying changes in each cover class (cf. Fig. 9a) with the average biomass for that class. This approach does not account for changes in non-woody (i.e., herbaceous) biomass, dead biomass, belowground biomass, and soil organic matter. Furthermore, the assumption that biomass increases or disappears in proportion with canopy cover certainly will often not hold at small scales, though it may be justified

Table 6
Summary of the extent and above-ground biomass (WAGB) carbon for woody vegetation in different woody cover fraction (WCF) classes. Also listed are changes in extent and total carbon between 2000 and 2018, and the mean biomass carbon density for each class. Carbon content was estimated as half of total dry matter.

WCF class	all	≥70 %	50–70 %	30–50 %	20–30 %	10–20 %	< 10 %
Extent in 2018 (10^6 ha)	531	12	14	33	41	73	357
Extent change 2000–2018 (10^6 ha)	−72	1	1	−6	−15	−46	−7
Biomass carbon density (tC ha^{-1})	12	95	90	50	23	12	2
Biomass carbon in 2018 (10^6 tC)	6596	1107	1223	1669	964	892	742
Biomass carbon change 2000–2018 (10^6 tC)	−1,050	130	50	−310	−345	−560	−14
Percentage of total woody vegetation extent (2018, %)	100 %	2%	3%	6%	8%	14 %	67 %
Percentage of biomass carbon (2018, %)	100 %	17 %	19 %	25 %	15 %	14 %	11 %

for total continental values.

The resulting calculation suggests that Australia lost 1.1 GtC in biomass between 2000–2018, corresponding to an average of 58.3 MtC y^{-1} or an equivalent emission of 214 Mt CO_2-eq y^{-1} (Table 6). This makes it a large, mostly additional, contribution to Australia's reported total annual emissions, which varied from 530 − 610 Mt CO_2-eq y^{-1} for the same period according to official Australian government reporting (Department of Environment and Energy, 2017). Vegetation biomass contributions from land use, land-use change and forestry (LULUCF) included in the official accounts represent only a small, and in recent years, negative (i.e. net uptake) component of reportable emissions. This is not necessarily inconsistent with the large emission source we infer, as the official inclusion of LULUCF biomass losses is subject to narrow definitions. Specifically, LULUCF reporting only includes change due to human activities, and the definition of forest applied in official statistics excludes any woody vegetation with less than 20 % forest canopy cover, whereas we found that this category was associated with 55 % of total carbon losses (Table 6). Regardless of these accounting conventions, our results indicate that the combined effects of drought mortality, bushfire and clearing in Australia's extensive areas of sparse woody vegetation have made a very large contribution to the country's total emissions. Whether these ecosystems will recover in future remains to be seen, given the persistent pressures of climate change and land use.

5. Conclusions

Our objective was to test whether machine learning can be used to combine multiple sources of spatial predictor and training data to estimate cover, height and biomass at high resolution across the Australian continent, where possible on an annual basis. We draw the following conclusions:

[1] Airborne LiDAR provided a rich source of training data to estimate cover and height from satellite optical, active radar and altimetry observations. The resulting predictions were of relatively high accuracy, explaining 89–94 % of the total variance, with estimation errors of 0.072 for cover fraction and 3.4 m for height, respectively.

[2] The use of annual Landsat surface reflectance geomedians was successful, and points at a way to achieve large-area high-resolution cover mapping that avoids the data quality and volume issues associated with the use of a single scene.

[3] The scarcity of ICESat/GLAS satellite LiDAR observations limited the achievable accuracy of tree height estimation, and through this, the estimation of biomass. The recent GEDI mission would appear to provide a valuable opportunity to improve this aspect of the methodology.

[4] Tree biomass could not be reliably predicted from satellite observations alone, but the inclusion of climate variables, in particular, mean temperature, led to considerably better accuracy. The overall accuracy was 80 t ha^{-1}, dominated by large unexplained variation for (tall) forests. While the plot biomass database provided a unique opportunity for the present study, the highly heterogeneous nature of these field-collected data also would have contributed to the unexplained variance.

[5] Preliminary interpretation of the cover time series demonstrated its suitability for detecting, and in some cases, attributing changes in woody cover. At the continental scale, the temporal dynamics of cover for the period 2000–2018 are primarily driven by changes in water availability and their effect on bush fires and mortality, particularly in sparse woody vegetation in Australia's drier interior.

[6] The importance of sparse woody ecosystems in Australia makes the estimation of total forest extent and even trends in extent susceptible to the tree cover fraction threshold chosen to define forests. This goes some way to explaining the divergence in published estimates. Comparison with categorical (as opposed to our continuous) forest cover mapping for four regions suggested that the cover data produced here can reliably be used for categorical forest cover mapping following any defined cover threshold.

[7] Loss of woody vegetation has made a very large contribution to Australia's total carbon emissions since 2000. Whether these ecosystems will recover biomass in future remains to be seen, given the persistent pressures of climate change and land use.

Author statement

Zhanmang Liao and Albert Van Dijk designed this study, carried out the analysis and wrote a first draft of the manuscript. Pablo Rozas Larraondo provided expert guidance in the use of the Random Forest algorithm, Peter Scarth provided expert guidance in the appropriate use of the in situ biomass data and radar and altimetry-based data and Binbin He provided support and mentoring to Zhanmang Liao; all three assisted in completing the manuscript.

CRediT authorship contribution statement

Zhanmang Liao: Conceptualization, Methodology, Software, Investigation, Data curation, Writing - review & editing. **Albert I.J.M. Van Dijk:** Conceptualization, Methodology, Software, Validation, Formal analysis, Writing - original draft, Supervision. **Binbin He:** Writing - review & editing, Funding acquisition. **Pablo Rozas Larraondo:** Resources, Writing - review & editing. **Peter F. Scarth:** Resources, Writing - review & editing.

Declaration of Competing Interest

The authors declare that they have no known competing financial interests or personal relationships that could have appeared to influence the work reported in this paper.

Acknowledgements

This research was made possible thanks to the collation of plot biomass data, the production of continental vegetation structure attributes, and the acquisition and processing of airborne LiDAR observations funded by the Terrestrial Ecosystem Research Network. Additional LiDAR data was acquired by the Australian Capital Territory

Government. High performance computing and data storage resources were made available by the National Computational Infrastructure. Z.L. was supported by a travel grant from the Chinese Science Council and the National Natural Science Foundation of China (Contract 41671361). We thank Drs Xingwen Quan, Marta Yebra and Xiangzhuo Liu for their assistance and companionship.

Appendix A. Supplementary data

Supplementary material related to this article can be found, in the online version, at doi:https://doi.org/10.1016/j.jag.2020.102209.

References

Baccini, A., et al., 2017. Tropical forests are a net carbon source based on aboveground measurements of gain and loss. Science 358 (6360), 230–234.
Department of Environment and Energy, 2017. Australian National Greenhouse Accounts: National Inventory Report, 2017 I.
Fisher, A., Armston, J., Goodwin, N., Scarth, P., 2020. Modelling canopy gap probability, foliage projective cover and crown projective cover from airborne lidar metrics in Australian forests and woodlands. Remote Sens. Environ. 237, 111520.
Furby, S., 2002. Land Cover Change: Specification for Remote Sensing Analysis. Australian Greenhouse Office, Canberra.
Guerschman, J.P., et al., 2015. Assessing the effects of site heterogeneity and soil properties when unmixing photosynthetic vegetation, non-photosynthetic vegetation and bare soil fractions from Landsat and MODIS data. Remote Sens. Environ. 161, 12–26.
Hansen, M.C., DeFries, R.S., Townshend, J.R.G., Sohlberg, R., 2000. Global land cover classification at 1 km spatial resolution using a classification tree approach. Int. J. Remote Sens. 21 (6), 1331–1364.
Hansen, M.C., et al., 2013. High-resolution global maps of 21st-century forest cover change. Science 342 (6160), 850–853.
Keith, H., Mackey, B.G., Lindenmayer, D.B., 2009. Re-evaluation of forest biomass carbon stocks and lessons from the world's most carbon-dense forests. Proc. Natl. Acad. Sci. U.S.A. 106 (28), 11635–11640.
Lefsky, M.A., et al., 2005. Estimates of forest canopy height and aboveground biomass using ICESat. Geophys. Res. Lett. 32 (22).
Lehmann, E.A., Wallace, J.F., Caccetta, P.A., Furby, S.L., Zdunic, K., 2013. Forest cover trends from time series Landsat data for the Australian continent. Int. J. Appl. Earth Obs. Geoinf. 21, 453–462.
Liu, Y.Y., et al., 2015. Recent reversal in loss of global terrestrial biomass. Nature Clim. Change 5 (5), 470–474.
Los, S., et al., 2012. Vegetation height products between 60° S and 60° N from ICESat GLAS data. Geosci. Model. Dev. 5, 413–432.
Lucas, R., et al., 2010. An evaluation of the ALOS PALSAR L-band backscatter—above ground biomass relationship Queensland, Australia: impacts of surface moisture condition and vegetation structure. IEEE J. Sel. Top. Appl. Earth Obs. Remote. Sens. 3 (4), 576–593.
Lucas, R., et al., 2012. Global forest monitoring with synthetic aperture radar (SAR) data. Global For. Monit. Earth Obs. 1, 287.
Nash, J.E., Sutcliffe, J.V., 1970. River flow forecasting through conceptual models part I — a discussion of principles. J. Hydrol. 10 (3), 282–290.
Roberts, D., Mueller, N., Mcintyre, A., 2017. High-dimensional pixel composites from earth observation time series. IEEE Trans. Geosci. Remote. Sens. 55 (11), 6254–6264.
Saatchi, S.S., et al., 2011. Benchmark map of forest carbon stocks in tropical regions across three continents. Proc. Natl. Acad. Sci.
Scarth, P., Armston, J., Lucas, R., Bunting, P., 2019. A structural classification of australian vegetation using ICESat/GLAS, ALOS PALSAR, and landsat sensor data. Remote Sens. 11 (2), 147.
Shimada, M., et al., 2014. New global forest/non-forest maps from ALOS PALSAR data (2007–2010). Remote Sens. Environ. 155, 13–31.
Simard, M., Pinto, N., Fisher, J.B., Baccini, A., 2011. Mapping forest canopy height globally with spaceborne lidar. J. Geophys. Res. Biogeosci. 116 (G4).
van Dijk, A.I.J.M., et al., 2013. The millennium drought in southeast Australia (2001–2009): natural and human causes and implications for water resources, ecosystems, economy and society. Water Resour. Res. 49, 1–18.
van Dijk, A., Mount, R., Gibbons, P., Vardon, M., Canadell, P., 2014. Environmental reporting and accounting in Australia: progress, prospects and research priorities. Sci. Total Environ. 473–474 (0), 338–349.
Van Dijk, A.I.J.M., Paget, M., Suarez, L., Gale, M., 2018. TERN Airborne LiDAR and Hyperspectral Products Document. Canberra. .
van Leeuwen, M., Nieuwenhuis, M., 2010. Retrieval of forest structural parameters using LiDAR remote sensing. Eur. J. For. Res. 129 (4), 749–770.
Wilson, J.P., Gallant, J.C., 2000. Secondary topographic attributes. Terrain anal. Principles appl. 87–131.